Changes in m^6A RNA methylation of goat lung following PPRV infection

Raja Ishaq Nabi Khan[1,2], Manas Ranjan Praharaj[3], Waseem Akram Malla[1], Neelima Hosamani[3], Shikha Saxena[1], Beena Mishra[4], Kaushal Kishor Rajak[4], Muthuchelvan Dhanavelu[5], B P Mishra[1,6,*], Basavaraj Sajjanar[1,*], Ravi Kumar Gandham[1,*]

1: Division of Veterinary Biotechnology, ICAR – Indian Veterinary Research Institute, Izatnagar Bareilly – 243122 (U.P., India)

2: Center for Advanced Biotechnology and Medicine, Rutgers University- 08854-8021(New Jersey, USA)

3: DBT- National Institute of Animal Biotechnology, Hyderabad – 500032 (Telangana, India)

4: Division of Biological Products, ICAR – Indian Veterinary Research Institute, Izatnagar Bareilly – 243122 (U.P., India)

5: Indian Veterinary Research Institute, Bengaluru Campus – 560024 (Karnatake, India)

6: ICAR – National Bureau of Animal Genetic Resources, Karnal – 132001 (Haryana, India)

*Corresponding authors: B P Mishra (bpmishra_1@hotmail.com), Basavaraj Sajjanar (basavaraj.sajjanar@icar.gov.in), Ravi Kumar Gandham (gandham71@gmail.com)

Abstract

Peste des petits ruminants (PPR) is an acute, highly contagious viral disease of goats and sheep, caused by the Peste des petits ruminants virus (PPRV). Earlier studies suggest the involvement of diverse regulatory mechanisms in PPRV infection. Methylation at N6 of Adenosine called m^6A is one such RNA modification that influences various physiological and pathological phenomena. As the lung tissue represents the primary target organ of PPRV, the present study explored the m^6A changes and their functional significance in PPRV disease pathogenesis. m^6A-seq analysis revealed 1289 m^6A peaks to be significantly altered in PPRV infected lung in comparison to normal lung, out of which 975 m^6A peaks were hypomethylated and 314 peaks were hypermethylated. Importantly, hypomethylated genes were enriched in Interleukin-4 and Interleukin-13 signaling and various processes associated with extracellular matrix organization. Further, of the 843 differentially m^6A containing genes, 282 genes were also found to be differentially expressed. Functional analysis revealed that these 282 genes are significantly enriched in signaling by Interleukins, extracellular matrix organization, cytokine signaling in the immune system, signaling by receptor tyrosine kinases, and Toll-like Receptor Cascades. We also found m^6A reader HNRNPC and the core

component of methyltransferase complex METTL14 to be highly upregulated than the m^6A readers – HNRNPA2B1 and YTHDF1 at the transcriptome level. These findings suggest that alteration in m^6A landscape following PPRV is implicated in diverse processes including the Interleukin signaling.

Keywords

Epitranscriptomics, m^6A, *Morbillivirus, Peste des petits ruminants virus*

Introduction

Peste des petits ruminants (PPR) is an acute, highly contagious viral disease of goats and sheep, caused by the Peste des petits ruminants virus (PPRV), a morbillivirus in the family Paramyxoviridae (Muthuchelvan, Rajak et al. 2015). PPR is characterized by mucous membrane congestion, pyrexia, pneumonia, nasal, ocular discharge, diarrhea, necrotic stomatitis, and leukopenia (Kumar, Tripathi et al. 2004). The disease is highly prevalent across sub-Saharan Africa, the Arabian Peninsula, and the Indian subcontinent (Banyard, Parida et al. 2010). Morbidity and mortality rates can reach 90-100% leading to severe economic losses in the endemic regions (Singh, De et al. 2010). Consequently, PPR has been classified as a World Organization for Animal Health (OIE) listed disease. The causative agent is a non-segmented RNA virus with a genome size of 15,948 nucleotides that encodes six structural proteins [nucleocapsid (N), phosphoprotein (P), matrix protein (M), fusion protein (F), haemagglutinin protein (H), and large protein (L)] in 3' to 5' direction and two non-structural proteins V and C resulting from the RNA editing of phosphoprotein (P) (Muthuchelvan, Rajak et al. 2015).

Various studies have been carried out to understand PPRV-host interactions, since the advent of next-generation sequencing, We previously studied the effect of the PPRV vaccine strain (Sungri/96) on goat PBMCs at the transcriptome level and reported a significant alteration in the expression of the genes involved in the regulation of innate immunity and apoptosis (Manjunath, Kumar et al. 2015). The dysregulation of innate immunity during PPRV infection of goat PBMCs has also been reported by a different group (Tirumurugaan, Pawar et al. 2020). In a virulent PPRV-host interactions study, lymphocytes have been observed to contribute more to counterattacking the PPRV infection whereas the contribution of monocytes was found to be limited (Wani, Sahu et al. 2019). The expression levels of viral

sensors and interferon-stimulated genes were found elevated only in lymphocytes following the viral infection (Wani, Sahu et al. 2019). Besides, the role of miRNAs in regulating PPRV infection has been reported (Pandey, Sahu et al. 2017, Khanduri, Sahu et al. 2018) suggestive of the involvement of diverse regulatory mechanisms in PPRV infection.

Epitranscriptomics (=RNA epigenetics) involves functionally relevant biochemical modifications of RNA taking place at the transcriptome level without a change in the sequence of ribonucleotides. More than 150 types of RNA modifications are present in different RNA types and among them, m^6A is most abundant in mRNAs and functionally well characterized (Boccaletto, Machnicka et al. 2018, Khan and Malla 2021). The enzymes that install the m^6A modification (=m^6A writers), that remove it (=m^6A erasers), and certain RNA binding proteins (=m^6A readers) that affect the fate of the m^6A-containing RNA by recruiting various proteins, have been found. m^6A influences RNA metabolism, which in turn influences various physiological and pathological conditions (He and He 2021). To identify the m^6A sites at the transcriptome level, antibody-based screening methods such as methylated RNA immunoprecipitation sequencing (meRIP-seq/m^6A-seq) are being widely used (Dominissini, Moshitch-Moshkovitz et al. 2012, Meyer, Saletore et al. 2012). RNA epigenetic changes are novel regulatory mechanisms that are strongly implicated in virus-host interactions. Zika Virus has been found to induce changes in m^6A modification of host RNA that affect translation, splicing, and mRNA stability (Lichinchi, Zhao et al. 2016). Similarly, HIV-1 Infection of T-cells has been found to influence the host mRNA methylomes (Lichinchi, Gao et al. 2016, Cristinelli, Angelino et al. 2021). KSHV(Kaposi's sarcoma-associated herpesvirus) latent infection regulates tumorigenic and epithelial-mesenchymal transition pathways by causing hypomethylation within 5′ untranslated region (UTR) and hypermethylation with 3′ UTR of host RNA (Tan, Liu et al. 2018). There have been no studies on the role of RNA modifications in the pathogenesis of PPRV in small ruminants. Further, insights into the pathobiology of PPRV could help in understanding the pathology of the related Measles virus.

The histological examination of the lungs of PPRV infected goats reveal proliferative changes like bronchitis, bronchiolitis, the proliferation of type II pneumocytes, and the presence of large multinucleated syncytial giant cells (Kumar, Tripathi et al. 2004, Chowdhury, Bhuiyan et al. 2014, Wani, Sahu et al. 2018). As the lung tissue represents the primary target organ of PPRV, the present study explored the epitranscriptomic changes and their functional significance in PPRV disease pathogenesis.

Methodology

Ethical Statement

The animals (n=2) used for the study were taken from the Indian Veterinary Research Institution (IVRI). The permission to conduct the study was granted by Institutional Animal Ethics Committee (IVRI-IAEC) under the Committee for Control and Supervision of Experiments on Animals (CPCSEA), India, vide letter no 387/CPSCEA. All relevant guidelines were followed for the study. The statement on ARRIVE guidelines followed for the study is enclosed as supplementary material.

Experimental animals and Sample collection

An overview of the experiment is shown in **Figure 1**. The experimental infection is part of the vaccine potency testing experiment. Goats (1 year of age) for the experiment were initially tested to be negative for the presence of PPRV antibodies by competitive ELISA (Singh, Sreenivasa et al. 2004) and serum neutralization test (Dhinakar Raj, Nachimuthu et al. 2000). A highly virulent PPRV (Izatnagar/94 - lineage IV; (Sahu, Wani et al. 2017)) isolate maintained at PPR Laboratory, Division of Virology, Indian Veterinary Research Institute, Mukteshwar was used as a challenge virus. A splenic suspension (10%) of the virulent virus was inoculated subcutaneously (4 ml suspension, 2 ml each at two different sites). The infected animals were sacrificed after they manifested the characteristic clinical symptoms of PPRV infection and lung tissue samples were collected (Pope, Parida et al. 2013). For this comparative study, lung samples of apparently healthy goats of the same age group were obtained from the nearby slaughterhouse as well. All the samples were stored in RNAlater RNA stabilizing solution(Qiagen, #76106) at 4 °C and then stored at – 80°C before proceeding further.

Sandwich ELISA (s-ELISA)

The samples were initially triturated in PBS followed by two cycles of freezing and thawing. s-ELISA of the supernatant collected was performed as per the instructions provided with the kit (Singh, Sreenivasa et al. 2004). Briefly, 100 µl capture antibody diluted in the ratio of 1:4000 was taken and then dispensed in all the wells of an ELISA plate. The ELISA plate was kept in the incubator on an orbital shaker at 37°C for incubation up to 1 h. At the end of incubation, the unbound antibodies were removed using the wash buffer composed of PBS and Tween-20. This step was repeated thrice. Thereafter, 50 µl of blocking buffer

(0.01M PBS containing 0.1% Tween-20? and 0.5% PPR negative goat serum) was added to all the wells of the ELISA plate. This was followed by the addition of the blocking buffer. The ELISA plate was kept in the incubator for 1 h at 37°C and thereafter the plate was washed. 100 µl of the primary antibody was added. This was followed by 1 h incubation at 37°C and washing. Diluted (1:1000) anti-mouse conjugate (100 µl) was added to all the wells of the plate. The ELISA plate was again kept in the incubator on an orbital shaker at 37°C for incubation up to 1 h. The discarding and washing procedures were repeated. 100 µl of OPD (o-phenylenediamine dihydrochloride) substrate solution was prepared. The solution was added to each well of the plate and the plate was kept in the incubator at 37°C for 10-20 minutes without shaking. The reaction was deemed to have completed when color developed in the positive reference (C+) wells. Thereafter, 100 µl stopping solution was dispensed in each well, and using an ELISA plate reader (Multiskan plus, LabSystem), the ELISA plate was read at 490 nm wavelength.

RT-PCR

RNA isolation was carried out using the Trizol method. Nanodrop (Thermo Scientific™) was used to measure the quantity of RNA and to assess protein and salt. The RNA integrity was assessed by running the RNA samples in TapeStation (Agilent). cDNA was prepared through PrimeScript™ 1st strand cDNA Synthesis Kit (cat #6110A). Diagnostic PCR for the N gene was carried out with the help of published primers (Couacy-Hymann, Roger et al. 2002). 10 µl of the reaction mixture was prepared with 5 µl of SapphireAmp Fast PCR Master Mix (Takara #RR350B), 1 µl of each of forward and reverse primers (final concentration 0.2 µM), 1 µl of 100ng template cDNA, and 2 µl of Nuclease Free Water (NFW). PCR was carried out with an initial denaturation at 95°C for 5 min followed by 35 cycles of denaturation at 95°C for 30 secs, annealing at 60°C for 30 secs, and renaturation at 72°C for 30 secs, with a final extension step at 72°C for 5 min. The PCR product was visualized on 1.5% agarose gel.

m^6A-sequencing

m^6A-seq was carried out as previously described (Dominissini, Moshitch-Moshkovitz et al. 2012) with minor chamnges .RNA of around 200 µg was fragmented using RNA fragmentation buffer (Merck #CS220011) at 94°C for 5 minutes. The fragmentation reaction was stopped by the addition of EDTA (Merck #CS203175). The purified fragmented RNA was precipitated by using Sodium Acetate (Sigma #S2889-250G), Glycogen, and 100%

ethanol. The size of the fragments was assessed through Tapestation. Around 100ng of the RNA was kept as input control and stored at -80°C whereas the remaining amount was subjected to immunoprecipitation using m^6A specific antibody (NEB #E1610S). Initially, 30 µg of Protein G magnetic beads (NEB #S1430) was washed with 250 µl of Immunoprecipitation Reaction Buffer (150 mM NaCl, 10 mM Tris-HCl, pH 7.5, 0.1% NP-40 in NFW) and using a magnetic rack (NEB #S1506), the buffer was decanted after equilibration. The step was repeated once. Then, 10 µl of m^6A antibody along with 200 ul Immunoprecipitation Reaction Buffer (IP) was added to the beads and incubated with head-over-tail rotation for 2 hours at 4°C. This was followed by the removal of the buffer by placing the microtube in a magnetic rack and three times washing with IP buffer. 200 µl IP buffer was along with fragmented RNA and 10 µl RNAse Inhibitor (Merck #CS216138) was then added to the antibody coupled to beads. The reaction mixture was incubated overnight at 4°C with head-over-tail rotation. This was followed by decanting off the buffer through the magnetic rack. The sample mixture was washed twice with 500 µl IP buffer, twice with low salt wash buffer (50 mM NaCl, 10 mM Tris-HCl, pH 7.5, 0.1% NP-40 in NFW), twice with high salt wash buffer (500 mM NaCl, 10 mM Tris-HCl, pH 7.5, 0.1% NP-40 in NFW), and once again with IP buffer. For elution of m^6A immunoprecipitated RNA, 100 µl of elution buffer [20mM m^6A Salt (Merck #CS220007) and IP Buffer] was added to the beads and incubated at 4°C with head-over-tail rotation for 1 hour. Thereafter, the elution buffer was transferred into a 1.5 ml microtube. The steps were repeated with another 100 ml volume of elution buffer. RNA was precipitated from a total of 200 µl of elution volume using ethanol, sodium acetate, and glycogen. RNA sequencing of the eluted RNA, as well as the input RNA, was carried out thereafter.

m^6A sequencing analysis

The sequencing reads were initially screened for their quality through FastQC software (Brown, Pirrung et al. 2017). Then, paired-end sequencing data of each sample was processed for the removal of adapters, low-quality reads, and singleton reads through Trimmomatic (Bolger, Lohse et al. 2014). The reference genome and the corresponding gtf file of *Capra hircus* (Bickhart, Rosen et al. 2017) were retrieved from Ensembl. Thereafter, paired-end data of each sample was mapped to the *Capra hircus* genome using HISAT2 (Wen 2017).. Samtools was used to convert sam files to bam format and to sort the bam files (Li, Handsaker et al. 2009). The PCR duplicates present in the bam files were removed through Picard tools. MeTDiff was used to find the m^6A peaks that vary between the infected

and non-infected samples with parameters: WINDOW_WIDTH=50, SLIDING_STEP=50, FRAGMENT_LENGTH=100, PEAK_CUTOFF_FDR=0.05, FOLD_ENRICHMENT=1 and DIFF_PEAK_CUTOFF_FDR=0.05 (Cui, Zhang et al. 2018). ChipSeekeer (Yu, Wang et al. 2015) was used to annotate m^6A peaks from the output bed files from MetDiff. Customized code was used to count the number of altered m^6A per gene and per chromosome. ggplot2 was used to plot figures.

RNA -sequencing analysis

The filtered sequencing data of the "INPUT RNA" of each sample was used for RNA-sequencing analysis. The reference genome was prepared and indexed by RNA-Seq by Expectation-Maximization (RSEM) by rsem-prepare-reference command (Li and Dewey 2011). Further, the clean reads obtained from filtering of raw data were aligned to the indexed reference genome by Bowtie2 (Langmead and Salzberg 2012) to estimate gene abundance in counts by rsem-calculate-expression command. To compare the gene expression levels between PPRV infective lung and PPRV negative lung, the aligned reads were used to generate a data matrix by 'rsem-generate-data-matrix' command and differential gene expression analysis was carried out by edgeR package (Robinson, McCarthy et al. 2010). The Ensembl IDs of the differentially expressed genes (DEGs) were converted to the respective gene ID by biomart (Durinck, Spellman et al. 2009), and the Reactome database was used for functional analysis (Fabregat, Jupe et al. 2018).

Real-time PCR

To validate the expression of the m^6A related enzymes, qRT-PCR was done. HMBS (Hydroxymethylbilane Synthase) was taken as the internal control as it was found to be the best suitable endogenous control in gene expression studies of PPRV infection in tissues(Sahu, Wani et al. 2018) . Each of the samples was run in triplicates and the relative expression of each gene was calculated using the $2^{-\Delta\Delta CT}$ method with control as the calibrator (Schmittgen and Livak 2008). . The student's t-test was done in JMP9 (SAS Institute Inc., Cary, USA) to test the significance of the difference. Differences between groups were considered significant at $P \leq 0.05$.

Results

Confirmation of the PPRV infection

PPRV specific N gene amplicon size of 351 bp confirmed the presence of PPRV infection in the lung of PPRV infected goats and the absence of PPRV in the lung of healthy goats. Sandwich ELISA revealed the absence of PPRV antigen in the tissue samples of apparently healthy goats and the presence of the PPRV antigen in the lung tissues of PPRV infected goats **(Supplementary File 1)**.

Alteration in m^6A Peaks in RNA of Lung of Goats under PPRV Infection

To find m^6A peaks that change under PPRV infection, m^6A seq data of infected lungs PPRV infected goat was compared with the lung of PPRV negative goat using MetDiff . m^6A-seq analysis revealed 1289 m^6A peaks to be significantly altered [FDR < 0.05, |FC| > 0.5] in PPRV infected lung in comparison to normal lung, out of which 975 m^6A peaks were hypomethylated [FDR < 0.05 , FC < –0.5] and 314 peaks were hypermethylated [FDR < 0.05, FC > +0.5] **(Supplementary File 2, Figure 2A, 2B).** As multiple m^6A peaks can be found in a single mRNA [13], expectedly, there can be alteration in m^6A peaks at more than one site within the same mRNA**.** A total of 1289 altered m^6A peaks were found to be distributed in the transcripts of 868 genes, out of which 643 genes contained only one altered m^6A peak, whereas 134 and 50 genes were found to change two and three positions respectively **(Figure 2C, Supplementary File 3).** We then investigated the distribution of the m^6A sites in the mRNA. Metaplot analysis revealed a higher distribution of m^6A peaks near the stop codon in the case of the control sample while a shift away from the stop codon was observed under PPRV infection. UTR regions remained unperturbed **(Figure 2D, 2E).** Chipseeker results revealed an equitable loss of m^6A peaks from UTRs and CDS (Relative loss of m^6A peaks = no. of hypomethylation/ total number of m^6A peaks) **(Figure 3A, 3B).** Overall, 32 genes were found to undergo hypomethylation as well as hypermethylation **(Figure 3C).** The distribution of differentially methylated m^6A containing genes across different chromosomes indicated relatively higher peaks in chromosomes 5, 13, and 19 **(Figure 3D)**.

Functional analysis of differentially m^6A containing genes

Through Reactome, we carried out functional analysis of the genes that had undergone only hypomethylation, only hypermethylation, and both hypermethylation as well as hypomethylation. We found out that hypermethylated genes are enriched for pathways that include PKMTs methylate histone lysines, synthesis of PIPs at the plasma membrane, RUNX1 regulates genes involved in megakaryocyte differentiation and platelet function,

Signaling by Interleukins, and TCF dependent signaling in response to WNT **(Figure 4A).** Hypomethylated genes were enriched in Interleukin-4 and Interleukin-13 signaling and various processes associated with extracellular matrix organization **(Figure 4C)**. The genes that undergo both hypomethylation as well as hypermethylation were found enriched in various RNA metabolic processes like mRNA editing, miRNA biogenesis, and repression and transcription regulation **(Figure 4B)**.

Functional analysis of differentially expressed genes

The input sequencing reads (INPUT RNA) of each sample were used for RNA sequencing analysis. The differential expression of genes in the lungs of PPRV infected animals in comparison to PPRV negative animals using edgeR revealed dysregulation of 5743 genes following PPRV infection, out of which 2547 were upregulated and 3196 were downregulated **(Supplementary File 4, Figure 5A, 5B)**. The upregulated genes were highly enriched in processes like neutrophil degranulation, rRNA modification in the nucleus and cytosol, Unfolded Protein Response (UPR), cellular response to heat stress, antiviral mechanism by IFN-stimulated genes, cytokine signaling in immune system, and signaling by Interleukins **(Figure 5C)** while downregulated genes were enriched in eukaryotic translation elongation, eukaryotic translation termination, viral mRNA Translation, nonsense-mediated decay, and extracellular matrix organization **(Figure 5D)**. We then looked into the genes related to the significant processes that were found to be enriched by the upregulated genes and downregulated genes (**Figure 5E)**.

Immune-related genes

In earlier studies of host-PPRV interaction, we have reported higher expression of genes encoding different molecule species such as Interferon-Stimulated Genes (ISGs), interleukins and viral sensors involved in innate immunity following PPRV infection (Wani, Sahu et al. 2019, Wani, Praharaj et al. 2021). Among the immune-related processes enriched by the upregulated genes, we found that upregulated genes involved in these processes are ISGs like *IFI44L, IFI6, IFIT1, IFIT2, IFIT3, IFIT5, IRF7, ISG15, ISG20,* and *MX1*; interleukin and interleukin receptors such as *IL17RA, IL18, IL1RN, IL4R, IL7R, IL10RB, IL17RB, IL1R2, IL1RL1, IL27, IL27RA, IL33,* and *IL6ST,* and viral sensors like RIG-I (*DDX58*), MDA5 (*IFIH1*) and *TLR2, TLR3, TLR4,* and *TLR6* **(Figure 5E)**.

Expression of Stress-related genes increased under PPRV infection

GPX and SOD are two components of the antioxidant triad that forms the first line of defence against reactive oxygen species (Bierl, Voetsch et al. 2004, Lee, Kim et al. 2008, Ighodaro and Akinloye 2018). The expression of GPX and SOD was found to increase following PPRV infection. Further, mRNAs encoding heat shock proteins such as heat shock protein HSP 90-alpha *(HSP90AA1*), heat shock 70 kDa protein 13 *(HSPA13)*, heat shock protein 105 kDa (*HSPH1*) were found to be elevated **(Figure 5E)**.

Expression of genes related to Extracellular matrix and RNA translation decreased under PPRV infection

Ribosomal proteins are vital for the translation of RNA. Few of the downregulated genes involved in the processes such as eukaryotic translation elongation, eukaryotic translation termination, viral mRNA included *RPLP1, RPS17, RPL35A, RPS21, RPL11,* and *RPL22*. Besides, certain downregulated genes involved in the extracellular matrix organization included Integrin alpha-D (*ITGAD)* and the *COL8A2, PHYKPL, LOXL1,* and *COL16A1* which are required for collagen synthesis **(Figure 5E)**.

We also screened the DEGs for the expression of known m^6A writers, readers, and erasers. We found m^6A reader *HNRNPC* and the core component of methyltransferase complex *METTL14* to be highly upregulated than the m^6A readers – *HNRNPA2B1* and *YTHDF1*. We also found the accessory component of METTL3/14 complex – *VIRMA* to be downregulated **(Figure 5F)**. The expression of VIRMA, METTL14, and YTHDF1 was confirmed through qPCR **(Supplementary File 5)**.

Correlation of DEGs with Differentially m^6A genes

m^6A modification influences the stability of the m^6A containing RNAs – it has been found to facilitate RNA degradation and stabilize the RNA as well and the process is contingent upon the location of m^6A on the transcript and the involvement of m^6A readers (Shi, Wang et al. 2017, Chen, Wei et al. 2018, Zhang, Kang et al. 2018, Lasman, Krupalnik et al. 2020). We, therefore, correlated the expression of DEGs with that of genes containing differential m^6A peaks. Of the 843 differentially m^6A containing genes, 282 genes were found to be differentially expressed. The 282 DEGs were categorized into 4 types of combinations 1) hypermethylated and upregulated genes 2) hypermethylated and downregulated 3) hypomethylated and upregulated genes 4) hypomethylated and downregulated genes. It was found that out of 282 DEGs, 103 downregulated genes were hypomethylated and 27 were hypermethylated. Also, 25 upregulated gene was found

hypermethylated and 116 were hypomethylated. Further, the proportion of DEGs that underwent a change in m^6A methylation at a single position was found far higher than the DEGs in which more than one m^6A methylation site changed following PPRV infection **(Figure 6A, 6B).** Functional analysis carried revealed that the 282 genes are significantly enriched in signaling by Interleukins, extracellular matrix organization, cytokine signaling in Immune system, signaling by receptor tyrosine kinases, and Toll-like Receptor Cascades **(Figure 6C)**. Among the interleukin family, a gain of m^6A methylation was found in upregulated mRNAs of interleukin receptors – *IL1R2* and *IL7R,* and the loss of m^6A methylation in upregulated *IL17RA* mRNA. Besides, loss of m^6A modification at three positions was found in downregulated mRNA of subunit A component of Complement C1q (*C1QA*). The only ISG in which there was a gain of m^6A was *OAS1*. Moreover, among the downregulated genes, genes involved in extracellular matrix organization – COL15A1, ITGA8, and LOXL1 were found to undergo loss of m^6A following PPRV infection. Moreover, loss of m^6A was also found in mRNA of upregulated HSP90 and HSP70 **(Figure 6D).**

Discussion

PPR is a contagious disease of sheep and goats. Because of wide geographical distribution with high mortality and morbidity, PPR is an economically important disease for small ruminant farming. Recently, high throughput techniques have been used for a better understanding of the molecular pathogenesis of PPRV. The immune mechanisms activated by the attenuated vaccine strain and virulent strains of PPRV indicate similar expression patterns (Manjunath, Kumar et al. 2015, Manjunath, Mishra et al. 2017, Wani, Sahu et al. 2019, Wani, Praharaj et al. 2021). However, differences in the degree of expression have been observed that pointed to the role of other regulatory mechanisms in PPRV infections.

We divulged one of the most abundant and functionally recognized RNA modifications – m^6A modification of host mRNA under PPRV infection. Goats were initially experimentally infected with the Izatnagar/94 strain (Sahu, Wani et al. 2017) of the virus and sacrificed following the development of the clinical presentation of PPRV infection on the 7th-day post-infection. Bilateral mucopurulent discharge, coughing, fetid diarrhea, and general weakness were observed (Pope, Parida et al. 2013). Among all the transcripts of PPRV, N mRNA is most transcribed and is used to confirm PPRV infection (Pandey, Sahu et al. 2017, Khanduri, Sahu et al. 2018, Wani, Sahu et al. 2019). Similarly, in the present study,

we confirmed experimental PPRV infection in goats using *N* gene expression and sandwich ELISA.

We carried out m^6A sequencing analysis of the infected samples as well as a noninfected sample (n=2) to identify the m^6A peaks that change following PPRV infection. 1289 m^6A peaks were found to be significantly altered in PPRV infected lungs in comparison to the control lungs. The results indicated a gain of m^6A as well as loss of m^6A taking place on mRNAs following PPRV infection. The significant alteration in the m^6A landscape of host mRNA has been reported in other m^6A studies of different host-viral interactions (Lichinchi, Zhao et al. 2016, Tan, Liu et al. 2018, Gokhale, McIntyre et al. 2020).

Our analysis revealed that the altered m^6A peaks represent transcripts of 868 genes. We found that certain mRNAs undergo m^6A change at more than one position, however, their proportion was lower as compared to those that change at a single point. In the case of the control lung, the m^6A peaks were found within the UTR and CDS regions but highly enriched near the stop codons as has been reported in other mammals (Dominissini, Moshitch-Moshkovitz et al. 2012). Earlier studies indicate that the change in the distribution of m^6A peaks can be virus-specific as well as cell-specific. The distribution of m^6A on host mRNA does not change following Zika virus, dengue virus, hepatitis C virus, and West Nile virus (Gokhale, McIntyre et al. 2020). Among the four different cell types infected with KSHV, a decrease within the 5' UTR and a corresponding increase within the 3' UTR was found in three cell types (Tan, Liu et al. 2018). However, no such redistribution of m^6A peaks of host mRNA after PPRV infection was found.

We also found that expression of m^6A writer METTL14 and an m^6A reader HNRNPC was elevated at the transcriptome level following PPRV infection. However, the expression of m^6A erasers FTO and ALKBH5 was found to be unperturbed. Thus, the cause-effect relation of the increase in the number of hypomethylated peaks with the expression of m^6A regulatory enzymes could not be linked in PPRV infected lungs. Recently transcription factors, histone modification, and RNA binding proteins have been found to regulate the recruitment of methyltransferase complex on target mRNAs (Barbieri, Tzelepis et al. 2017, Fish, Navickas et al. 2019, Huang, Weng et al. 2019). Moreover, a decrease in transcriptional rate has been shown to increase the number of m^6A sites (Slobodin, Han et al. 2017). The intricate influence of various accessory factors could also influence alteration in m^6A peaks following PPRV infection.

Functional analysis of upregulated genes showed enrichment in IFN-stimulated genes, cytokine signaling in immune system, and signaling by Interleukins. Notable upregulated

genes involved in these are ISGs, interleukin and interleukin receptors, and viral sensors. ISGs – ISG15, ISG20, IRF7, IFIT1, IFIT3, IFIT5, MX1, IFI6, and OAS1 whose antiviral activity has been reported in various RNA virus infections (Schneider, Chevillotte et al. 2014), have also been found to be elevated in lymphocytes isolated from virulent PPRV infected goat (Wani, Sahu et al. 2019) and various PBMCs subsets isolated from Sungri 96/PPRV vaccine goats (Wani, Praharaj et al. 2021).

The expression pattern of viral sensors RIG-I and MDA5 which are required for stimulation of ISGs (Park, Iwasaki et al. 2020) is similar to virulent PPRV infected lymphocytes (Wani, Sahu et al. 2019) and PBMCs from PPRV vaccinated animals (Wani, Praharaj et al. 2021). Moreover, upregulated genes were also found enriched in stress response genes. The molecules involved are antioxidants – SOD2 and GPX2 which alleviate the virus-induced oxidative injury (Camini, da Silva Caetano et al. 2017). Ribosomal proteins like RPLP1, RPS17, RPL11, and RPL22 which have a positive influence on viral propagation are downregulated (Belhadj Slimen, Najar et al. 2014).

We also found that hypermethylated transcripts were enriched in processes that are associated with chromosomal organization, synthesis of PIPs at the plasma membrane, megakaryocyte differentiation and platelet function, Interleukin signaling, and WNT signaling. The hypomethylated genes were associated specifically with Interleukin-4 and Interleukin-13 signaling and various processes associated with extracellular matrix organization. The alteration in m^6A under PPRV infection is not just limited to transcripts of specific processes or signaling but ranges from different innate immune processes to the processes related to cell proliferation and extracellular organization. m^6A regulates RNA stability, RNA translation, splicing, and export from the nucleus (He and He 2021). To analyze the effect of altered m^6A modification on gene expression, we correlated the RNA sequencing data with m^6A-seq data. Both loss and gain of m^6A modification were found in upregulated as well as downregulated genes, which is in coherence with the studies about stabilizing as well as the destabilizing effect of m^6A (Shi, Wang et al. 2017, Chen, Wei et al. 2018, Zhang, Kang et al. 2018, Lasman, Krupalnik et al. 2020). We found that the proportion of hypomethylated downregulated and hypomethylated upregulated is very high than the proportion of hypermethylated downregulated and hypermethylated upregulated. No change in m^6A was found in upregulated mRNAs of ISGs, interleukins, and viral sensors. However, upregulated genes of interleukin receptors such as IL1R2, I L7R and *IL17RA* were found where an alteration in m^6A sites was found. m^6A modification seems to play an important role in regulating interleukin expression and ISG expression during PPRV.

Conclusion

Through m^6A-seq analysis of lung of goat, m^6A peaks were found to be significantly altered following PPRV infection. The m^6A hypomethylated genes were found enriched in Interleukin-4 and Interleukin-13 signaling. A fraction of differentially expressed genes in which alteration of m^6A modification was found belong to cytokine signaling pathway. The involvement of m^6A modification adds another connecting link between the PPRV infection and the host.

Legends

1. **Workflow for m^6A sequencing analysis and RNA sequencing analysis**

2. **Change in m^6A peaks following PPRV infection (A)** Volcano Plot of differentially methylated genes in lung PPRV infection. The X-axis is the log2ratio of methylation level between the infected and control lung. The Y-axis is the differential FDR based on a negative log scale. The cyan dots represent the significant differential m^6A peaks, based on FDR< 0.05 and |FC| > 0.5. (B) Bar diagram showing the number of hypomethylated and hypermethylated m^6A peaks (C) The distribution of differential m^6A peaks per gene (D) Metaplot of m^6A peaks in control lung (E) Metaplot of m^6A peaks in PPRV infected lung

3. (A) The number of altered m^6A peaks in CDS and UTR regions (B) Relative loss of m^6A peaks (= no. of hypomethylation/ total number of altered m^6A peaks *100) from UTR and CDS region (C) Venn diagram showing the genes that are hypermethylated at a certain position(s) and hypomethylated at other position(s) (D) Distribution of hypomethylated and hypermethylated m^6A peaks in different chromosomes.

4. The functional analysis of genes with (A) m^6A hypermethylated (C) m^6A hypomethylated peaks (B) having both hypermethylated and hypomethylated peaks. The significance of the process is based on p-value as indicated by –log10 (P) on X-axis.

5. **Change in expression of genes following PPRV infection** (A) Volcano Plot of differentially expressed genes in the spleen following PPRV infection. The X-axis is the log2 ratio of expression level between the infected and control lung. The Y-axis is the differential FDR based on negative log scale. The cyan dots represent significant DEGs based on FDR < 0.05 and |FC| > 0.5 (B) The number of upregulated and downregulated m^6A peaks (C) Functional analysis of upregulated genes (D) Functional analysis of downregulated genes. The significance of the process in figures (C) and (D) is based on p-value as indicated by –log10 (P) on the left Y-axis. The right Y-axis in Figures (C) and (D) indicate the number of genes involved in the processes. (E) Alteration in expression of enzymes related to m6A regulatory

machinery. (F) Log_2FC of genes involved in the different processes associated with DEGs. The red color indicates upregulated genes and the green color indicates downregulated genes

6. **Correlation between differential m^6A-containing peaks and differentially expressed genes: (A)** The changes in m^6A peaks of differentially expressed genes: total, at one position ($1dm^6A$), and at two positions ($2dm^6A$). The combinations shown include Hypermethylated and upregulated genes; Hypermethylated and downregulated; Hypomethylated and upregulated genes, and Hypomethylated and downregulated genes in the lung following PPRV infection. (B) Quadrant plots of differentially expressed genes in which there was alteration at one site. The X-axis is the log2 ratio of methylation level between the infected and control tissue. The Y-axis is the log2 ratio of expression level between the infected and control tissue (C) Functional analysis of the DEGs which contain differential m^6A peaks (D) Log2FC values of change in methylation and expression of some important genes

References

Banyard, A. C., S. Parida, C. Batten, C. Oura, O. Kwiatek and G. J. J. o. g. v. Libeau (2010). "Global distribution of peste des petits ruminants virus and prospects for improved diagnosis and control." **91**(12): 2885-2897.

Barbieri, I., K. Tzelepis, L. Pandolfini, J. Shi, G. Millán-Zambrano, S. C. Robson, D. Aspris, V. Migliori, A. J. Bannister, N. Han, E. De Braekeleer, H. Ponstingl, A. Hendrick, C. R. Vakoc, G. S. Vassiliou and T. Kouzarides (2017). "Promoter-bound METTL3 maintains myeloid leukaemia by m(6)A-dependent translation control." Nature **552**(7683): 126-131.

Belhadj Slimen, I., T. Najar, A. Ghram, H. Dabbebi, M. Ben Mrad and M. Abdrabbah (2014). "Reactive oxygen species, heat stress and oxidative-induced mitochondrial damage. A review." International journal of hyperthermia **30**(7): 513-523.

Bickhart, D. M., B. D. Rosen, S. Koren, B. L. Sayre, A. R. Hastie, S. Chan, J. Lee, E. T. Lam, I. Liachko and S. T. J. N. g. Sullivan (2017). "Single-molecule sequencing and chromatin conformation capture enable de novo reference assembly of the domestic goat genome." **49**(4): 643-650.

Bierl, C., B. Voetsch, R. C. Jin, D. E. Handy and J. Loscalzo (2004). "Determinants of human plasma glutathione peroxidase (GPx-3) expression." Journal of Biological Chemistry **279**(26): 26839-26845.

Boccaletto, P., M. A. Machnicka, E. Purta, P. Piątkowski, B. Bagiński, T. K. Wirecki, V. de Crécy-Lagard, R. Ross, P. A. Limbach and A. J. N. a. r. Kotter (2018). "MODOMICS: a database of RNA modification pathways. 2017 update." **46**(D1): D303-D307.

Bolger, A. M., M. Lohse and B. J. B. Usadel (2014). "Trimmomatic: a flexible trimmer for Illumina sequence data." **30**(15): 2114-2120.

Brown, J., M. Pirrung and L. A. J. B. McCue (2017). "FQC Dashboard: integrates FastQC results into a web-based, interactive, and extensible FASTQ quality control tool." **33**(19): 3137-3139.

Camini, F. C., C. C. da Silva Caetano, L. T. Almeida and C. L. de Brito Magalhães (2017). "Implications of oxidative stress on viral pathogenesis." Archives of Virology **162**(4): 907-917.

Chen, M., L. Wei, C. T. Law, F. H. Tsang, J. Shen, C. L. Cheng, L. H. Tsang, D. W. Ho, D. K. Chiu, J. M. Lee, C. C. Wong, I. O. Ng and C. M. Wong (2018). "RNA N6-methyladenosine methyltransferase-like 3 promotes liver cancer progression through YTHDF2-dependent posttranscriptional silencing of SOCS2." **67**(6): 2254-2270.

Chowdhury, E. H., A. R. Bhuiyan, M. M. Rahman, M. S. A. Siddique and M. R. J. B. V. R. Islam (2014). "Natural peste des petits ruminants virus infection in Black Bengal goats: virological, pathological and immunohistochemical investigation." **10**(1): 1-10.

Couacy-Hymann, E., F. Roger, C. Hurard, J. Guillou, G. Libeau and A. J. J. o. v. m. Diallo (2002). "Rapid and sensitive detection of peste des petits ruminants virus by a polymerase chain reaction assay." **100**(1-2): 17-25.

Cristinelli, S., P. Angelino, A. Janowczyk, M. Delorenzi and A. J. b. Ciuffi (2021). "HIV modifies the m6A and m5C epitranscriptomic landscape of the host cell." 2021.2001. 2004.425358.

Cui, X., L. Zhang, J. Meng, M. K. Rao, Y. Chen and Y. Huang (2018). "MeTDiff: A Novel Differential RNA Methylation Analysis for MeRIP-Seq Data." IEEE/ACM Trans Comput Biol Bioinform **15**(2): 526-534.

Dhinakar Raj, G., K. Nachimuthu and A. Mahalinga Nainar (2000). "A simplified objective method for quantification of peste des petits ruminants virus or neutralizing antibody." J Virol Methods **89**(1-2): 89-95.

Dominissini, D., S. Moshitch-Moshkovitz, S. Schwartz, M. Salmon-Divon, L. Ungar, S. Osenberg, K. Cesarkas, J. Jacob-Hirsch, N. Amariglio and M. Kupiec (2012). "Topology of the human and mouse m 6 A RNA methylomes revealed by m 6 A-seq." Nature **485**(7397): 201-206.

Durinck, S., P. T. Spellman, E. Birney and W. J. N. p. Huber (2009). "Mapping identifiers for the integration of genomic datasets with the R/Bioconductor package biomaRt." **4**(8): 1184.

Fabregat, A., S. Jupe, L. Matthews, K. Sidiropoulos, M. Gillespie, P. Garapati, R. Haw, B. Jassal, F. Korninger and B. J. N. a. r. May (2018). "The reactome pathway knowledgebase." **46**(D1): D649-D655.
Fish, L., A. Navickas, B. Culbertson, Y. Xu, H. C. Nguyen, S. Zhang, M. Hochman, R. Okimoto, B. D. Dill and H. J. M. c. Molina (2019). "Nuclear TARBP2 drives oncogenic dysregulation of RNA splicing and decay." **75**(5): 967-981. e969.
Gokhale, N. S., A. B. McIntyre, M. D. Mattocks, C. L. Holley, H. M. Lazear, C. E. Mason and S. M. J. M. c. Horner (2020). "Altered m6A modification of specific cellular transcripts affects Flaviviridae infection." **77**(3): 542-555. e548.
He, P. C. and C. J. T. E. J. He (2021). "m6A RNA methylation: from mechanisms to therapeutic potential." **40**(3): e105977.
Huang, H., H. Weng, K. Zhou, T. Wu, B. S. Zhao, M. Sun, Z. Chen, X. Deng, G. Xiao, F. Auer, L. Klemm, H. Wu, Z. Zuo, X. Qin, Y. Dong, Y. Zhou, H. Qin, S. Tao, J. Du, J. Liu, Z. Lu, H. Yin, A. Mesquita, C. L. Yuan, Y. C. Hu, W. Sun, R. Su, L. Dong, C. Shen, C. Li, Y. Qing, X. Jiang, X. Wu, M. Sun, J. L. Guan, L. Qu, M. Wei, M. Müschen, G. Huang, C. He, J. Yang and J. Chen (2019). "Histone H3 trimethylation at lysine 36 guides m(6)A RNA modification co-transcriptionally." Nature **567**(7748): 414-419.
Ighodaro, O. and O. Akinloye (2018). "First line defence antioxidants-superoxide dismutase (SOD), catalase (CAT) and glutathione peroxidase (GPX): Their fundamental role in the entire antioxidant defence grid." Alexandria Journal of Medicine **54**(4): 287-293.
Khan, R. I. N. and W. A. Malla (2021). "m6A modification of RNA and its role in cancer, with a special focus on lung cancer." Genomics.
Khanduri, A., A. R. Sahu, S. A. Wani, R. I. N. Khan, A. Pandey, S. Saxena, W. A. Malla, P. Mondal, K. K. Rajak and B. Mishra (2018). "Dysregulated miRNAome and proteome of PPRV infected goat PBMCs reveal a coordinated immune response." Frontiers in immunology **9**: 2631.
Kumar, P., B. Tripathi, A. Sharma, R. Kumar, B. Sreenivasa, R. Singh, P. Dhar and S. J. J. o. V. M. Bandyopadhyay, Series B (2004). "Pathological and immunohistochemical study of experimental peste des petits ruminants virus infection in goats." **51**(4): 153-159.
Langmead, B. and S. L. Salzberg (2012). "Fast gapped-read alignment with Bowtie 2." Nature methods **9**(4): 357.
Lasman, L., V. Krupalnik, S. Geula, M. Zerbib, S. Viukov, N. Mor, A. Aguilera, O. Mizrahi, S. Shashank and A. Nachshon (2020). "Context-dependent functional compensation between Ythdf m6A readers." bioRxiv.
Lee, Y. S., A. Y. Kim, J. W. Choi, M. Kim, S. Yasue, H. J. Son, H. Masuzaki, K. S. Park and J. B. Kim (2008). "Dysregulation of adipose glutathione peroxidase 3 in obesity contributes to local and systemic oxidative stress." Molecular Endocrinology **22**(9): 2176-2189.
Li, B. and C. N. Dewey (2011). "RSEM: accurate transcript quantification from RNA-Seq data with or without a reference genome." BMC bioinformatics **12**(1): 323.
Li, H., B. Handsaker, A. Wysoker, T. Fennell, J. Ruan, N. Homer, G. Marth, G. Abecasis and R. J. B. Durbin (2009). "The sequence alignment/map format and SAMtools." **25**(16): 2078-2079.
Lichinchi, G., S. Gao, Y. Saletore, G. M. Gonzalez, V. Bansal, Y. Wang, C. E. Mason and T. M. J. N. m. Rana (2016). "Dynamics of the human and viral m 6 A RNA methylomes during HIV-1 infection of T cells." **1**(4): 1-9.
Lichinchi, G., B. S. Zhao, Y. Wu, Z. Lu, Y. Qin, C. He, T. M. J. C. h. Rana and microbe (2016). "Dynamics of human and viral RNA methylation during Zika virus infection." **20**(5): 666-673.
Manjunath, S., G. R. Kumar, B. P. Mishra, B. Mishra, A. P. Sahoo, C. G. Joshi, A. K. Tiwari, K. K. Rajak and S. C. J. V. r. Janga (2015). "Genomic analysis of host–Peste des petits ruminants vaccine viral transcriptome uncovers transcription factors modulating immune regulatory pathways." **46**(1): 1-15.
Manjunath, S., B. P. Mishra, B. Mishra, A. P. Sahoo, A. K. Tiwari, K. K. Rajak, D. Muthuchelvan, S. Saxena, L. Santra and A. R. Sahu (2017). "Comparative and temporal transcriptome analysis of peste des petits ruminants virus infected goat peripheral blood mononuclear cells." Virus research **229**: 28-40.

Meyer, K. D., Y. Saletore, P. Zumbo, O. Elemento, C. E. Mason and S. R. Jaffrey (2012). "Comprehensive analysis of mRNA methylation reveals enrichment in 3' UTRs and near stop codons." Cell **149**(7): 1635-1646.
Muthuchelvan, D., K. Rajak, M. Ramakrishnan, D. Choudhary, S. Bhadouriya, P. Saravanan, A. Pandey and R. J. A. A. V. S. Singh (2015). "Peste-des-petits-ruminants: An Indian perspective." **3**(8): 422-429.
Pandey, A., A. R. Sahu, S. A. Wani, S. Saxena, S. Kanchan, V. Sah, K. K. Rajak, A. Khanduri, A. P. Sahoo and A. K. Tiwari (2017). "Modulation of host miRNAs transcriptome in lung and spleen of Peste des Petits ruminants virus infected sheep and goats." Frontiers in microbiology **8**: 1146.
Park, A., A. J. C. h. Iwasaki and microbe (2020). "Type I and type III interferons–induction, signaling, evasion, and application to combat COVID-19."
Pope, R. A., S. Parida, D. Bailey, J. Brownlie, T. Barrett and A. C. J. P. o. Banyard (2013). "Early events following experimental infection with peste-des-petits ruminants virus suggest immune cell targeting." **8**(2): e55830.
Robinson, M. D., D. J. McCarthy and G. K. Smyth (2010). "edgeR: a Bioconductor package for differential expression analysis of digital gene expression data." Bioinformatics **26**(1): 139-140.
Sahu, A. R., S. A. Wani, M. Saminathan, K. K. Rajak, A. P. Sahoo, A. Pandey, S. Saxena, S. Kanchan, A. K. Tiwari and B. J. A. o. v. Mishra (2017). "Genome sequencing of an Indian peste des petits ruminants virus isolate, Izatnagar/94, and its implications for virus diversity, divergence and phylogeography." **162**(6): 1677-1693.
Sahu, A. R., S. A. Wani, S. Saxena, K. K. Rajak, D. Chaudhary, A. P. Sahoo, A. Khanduri, A. Pandey, P. Mondal and W. A. J. S. r. Malla (2018). "Selection and validation of suitable reference genes for qPCR gene expression analysis in goats and sheep under Peste des petits ruminants virus (PPRV), lineage IV infection." **8**(1): 1-11.
Schmittgen, T. D. and K. J. Livak (2008). "Analyzing real-time PCR data by the comparative C T method." Nature protocols **3**(6): 1101.
Schneider, W. M., M. D. Chevillotte and C. M. J. A. r. o. i. Rice (2014). "Interferon-stimulated genes: a complex web of host defenses." **32**: 513-545.
Shi, H., X. Wang, Z. Lu, B. S. Zhao, H. Ma, P. J. Hsu, C. Liu and C. He (2017). "YTHDF3 facilitates translation and decay of N 6-methyladenosine-modified RNA." Cell research **27**(3): 315-328.
Singh, R., U. De, K. J. C. i. Pandey, microbiology and i. diseases (2010). "Virological and antigenic characterization of two peste des petits ruminants (PPR) vaccine viruses of Indian origin." **33**(4): 343-353.
Singh, R. P., B. P. Sreenivasa, P. Dhar and S. K. Bandyopadhyay (2004). "A sandwich-ELISA for the diagnosis of Peste des petits ruminants (PPR) infection in small ruminants using anti-nucleocapsid protein monoclonal antibody." Arch Virol **149**(11): 2155-2170.
Singh, R. P., B. P. Sreenivasa, P. Dhar, L. C. Shah and S. K. Bandyopadhyay (2004). "Development of a monoclonal antibody based competitive-ELISA for detection and titration of antibodies to peste des petits ruminants (PPR) virus." Vet Microbiol **98**(1): 3-15.
Slobodin, B., R. Han, V. Calderone, J. A. O. Vrielink, F. Loayza-Puch, R. Elkon and R. Agami (2017). "Transcription impacts the efficiency of mRNA translation via co-transcriptional N6-adenosine methylation." Cell **169**(2): 326-337. e312.
Tan, B., H. Liu, S. Zhang, S. R. da Silva, L. Zhang, J. Meng, X. Cui, H. Yuan, O. Sorel and S.-W. J. N. m. Zhang (2018). "Viral and cellular N 6-methyladenosine and N 6, 2′-O-dimethyladenosine epitranscriptomes in the KSHV life cycle." **3**(1): 108-120.
Tirumurugaan, K. G., R. M. Pawar, G. Dhinakar Raj, A. Thangavelu, J. A. Hammond and S. J. V. Parida (2020). "RNAseq Reveals the Contribution of Interferon Stimulated Genes to the Increased Host Defense and Decreased PPR Viral Replication in Cattle." **12**(4): 463.
Wani, S. A., M. R. Praharaj, A. R. Sahu, R. I. N. Khan, S. Saxena, K. K. Rajak, D. Muthuchelvan, A. Sahoo, B. Mishra and R. K. J. M. Singh (2021). "Systems Biology behind immunoprotection of both Sheep and Goats after Sungri/96 PPRV vaccination." **6**(2).

Wani, S. A., A. R. Sahu, R. I. N. Khan, A. Pandey, S. Saxena, N. Hosamani, W. A. Malla, D. Chaudhary, S. Kanchan and V. Sah (2019). "Contrasting gene expression profiles of monocytes and lymphocytes from Peste-des-petits-ruminants virus infected goats." Frontiers in Immunology **10**.

Wani, S. A., A. R. Sahu, S. Saxena, K. K. Rajak, M. Saminathan, A. P. Sahoo, S. Kanchan, A. Pandey, B. Mishra and D. J. M. p. Muthuchelvan (2018). "Expression kinetics of ISG15, IRF3, IFNγ, IL10, IL2 and IL4 genes vis-a-vis virus shedding, tissue tropism and antibody dynamics in PPRV vaccinated, challenged, infected sheep and goats." **117**: 206-218.

Wen, G. (2017). A simple process of RNA-sequence analyses by Hisat2, Htseq and DESeq2. Proceedings of the 2017 International Conference on Biomedical Engineering and Bioinformatics.

Yu, G., L.-G. Wang and Q.-Y. J. B. He (2015). "ChIPseeker: an R/Bioconductor package for ChIP peak annotation, comparison and visualization." **31**(14): 2382-2383.

Zhang, F., Y. Kang, M. Wang, Y. Li, T. Xu, W. Yang, H. Song, H. Wu, Q. Shu and P. Jin (2018). "Fragile X mental retardation protein modulates the stability of its m6A-marked messenger RNA targets." Human Molecular Genetics **27**(22): 3936-3950.

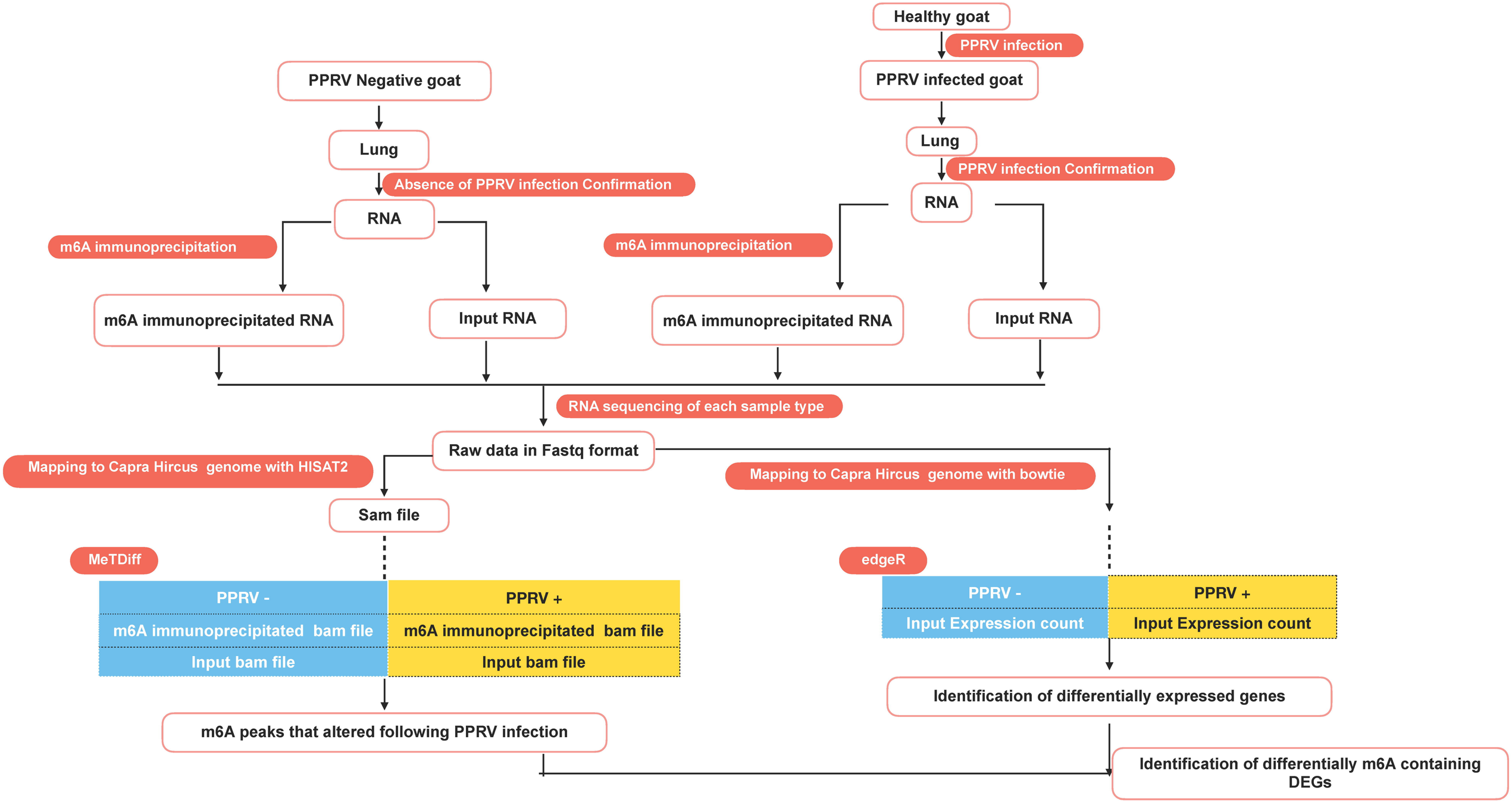
Healthy goat
PPRV infection
PPRV infected goat
PPRV Negative goat
Lung
Lung
PPRV infection Confirmation
Absence of PPRV infection Confirmation
RNA
RNA
m6A immunoprecipitation
m6A immunoprecipitation
m6A immunoprecipitated RNA
Input RNA
m6A immunoprecipitated RNA
Input RNA
RNA sequencing of each sample type
Raw data in Fastq format
Mapping to Capra Hircus genome with HISAT2
Mapping to Capra Hircus genome with bowtie
Sam file
MeTDiff
edgeR
PPRV -
PPRV +
m6A immunoprecipitated bam file
m6A immunoprecipitated bam file
Input bam file
Input bam file
PPRV -
PPRV +
Input Expression count
Input Expression count
Identification of differentially expressed genes
m6A peaks that altered following PPRV infection
Identification of differentially m6A containing DEGs

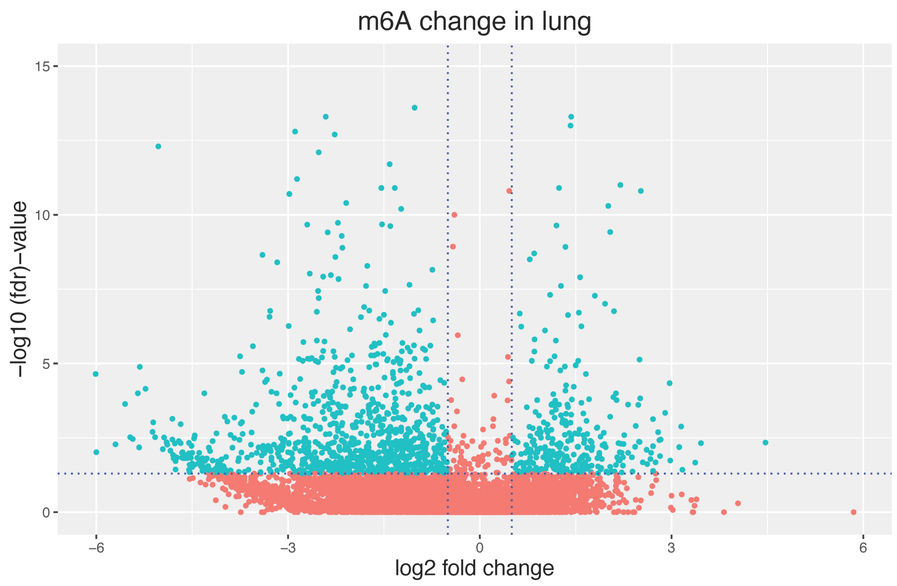
m6A change in lung
−log10 (fdr)−value
log2 fold change
15
10
5
0
−6
−3
0
3
6

(A)

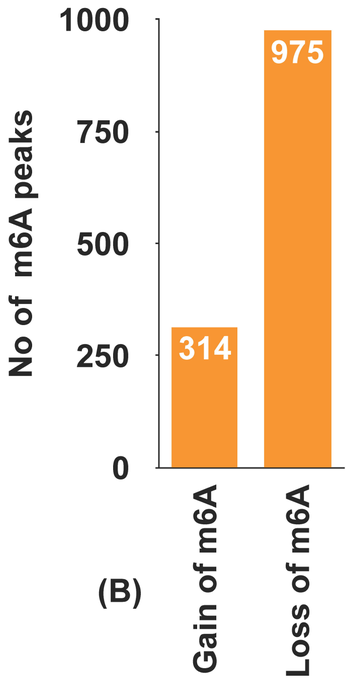
No of m6A peaks
1000
750
500
250
0
975
314
Gain of m6A
Loss of m6A

(B)

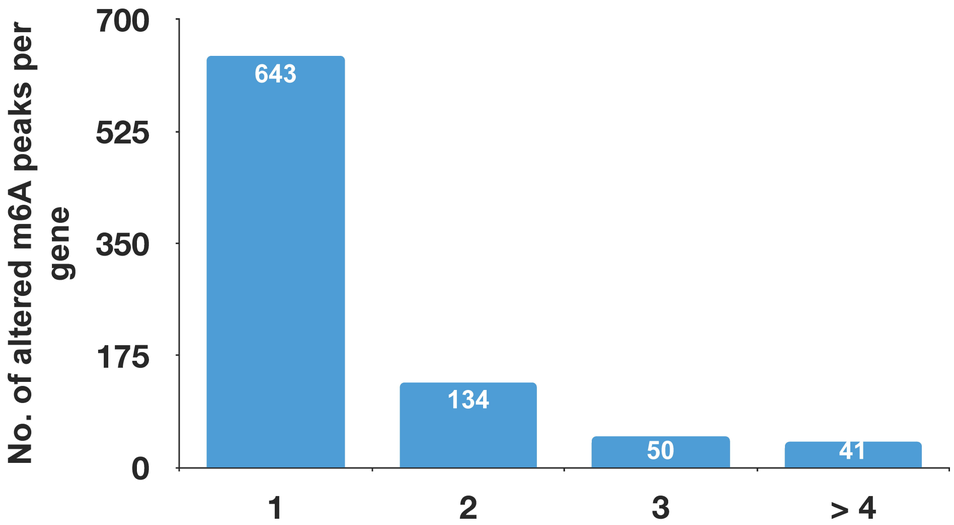
No. of altered m6A peaks per gene
700
525
350
175
0
643
134
50
41
1
2
3
> 4

(C)

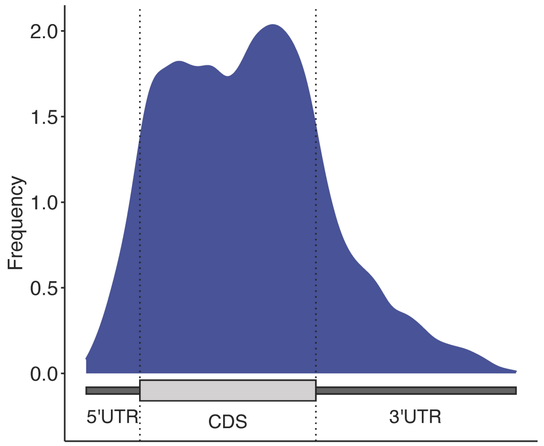
Frequency
2.0
1.5
1.0
0.5
0.0
5'UTR
CDS
3'UTR

(D)

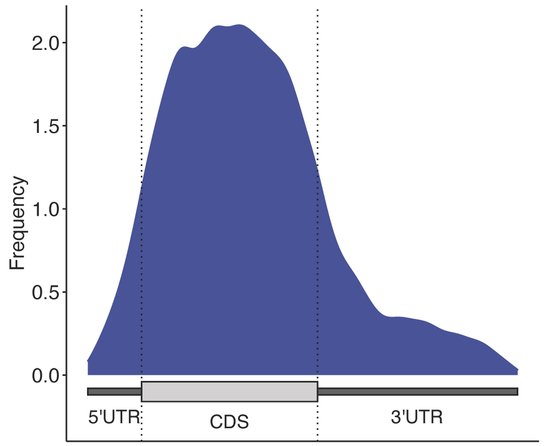
Frequency
2.0
1.5
1.0
0.5
0.0
5'UTR
CDS
3'UTR

(E)

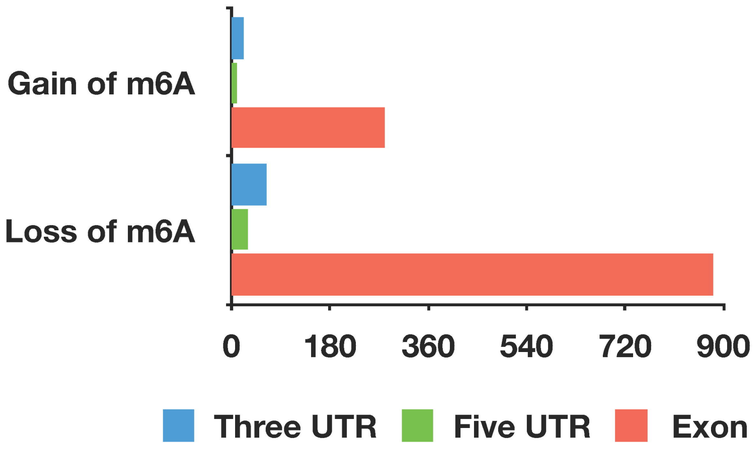
Gain of m6A
Loss of m6A
0
180
360
540
720
900
Three UTR
Five UTR
Exon

(A)

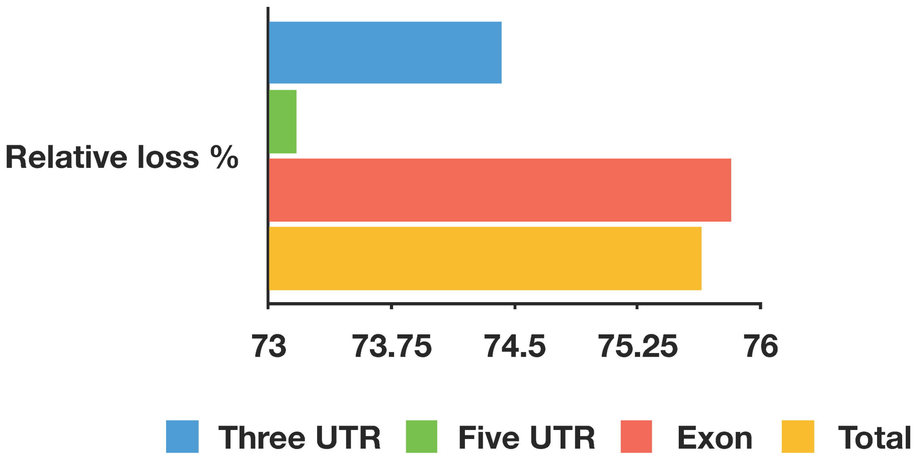
Relative loss %
73
73.75
74.5
75.25
76
Three UTR
Five UTR
Exon
Total

(B)

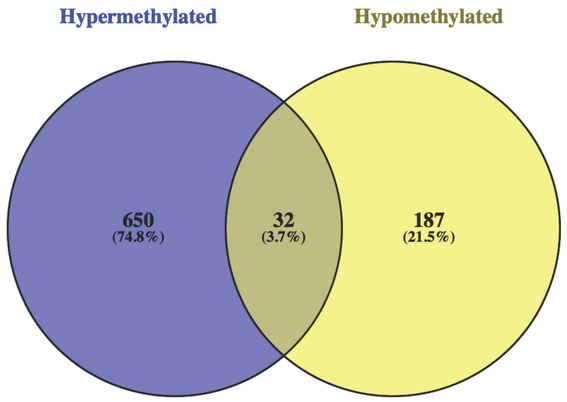
Hypermethylated
Hypomethylated
650
(74.8%)
32
(3.7%)
187
(21.5%)

(C)

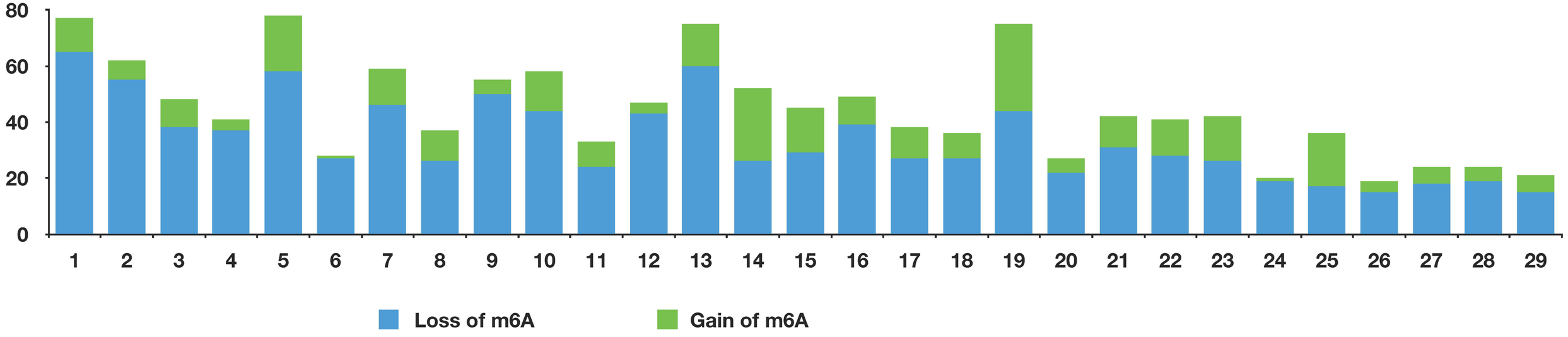
80
60
40
20
0
1
2
3
4
5
6
7
8
9
10
11
12
13
14
15
16
17
18
19
20
21
22
23
24
25
26
27
28
29
Loss of m6A
Gain of m6A

(D)

Only hypermethylated genes

(A)

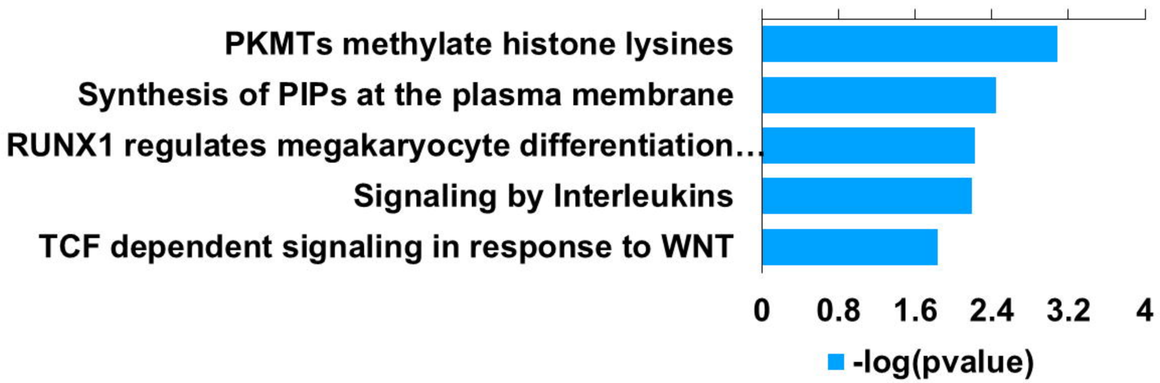

ATF7IP	*KMT2D*	*MECOM*	*SETD1B*	*H3C12*
MTMR3	*PIP5K1B*	*PIK3C2A*	*PIK3R5*	*SIN3A*
RUNX1	*HSPA8*	*SMAD3*	*CISH*	*MYC*
IL1R2	*PITPNA*	*CSF2RB*	*GAB2*	*IL7R*
TNFRSF1B	*IL18BP*	*BCL9*	*CHD8*	

Hypermethylated as well as hypomethylated genes

(C)

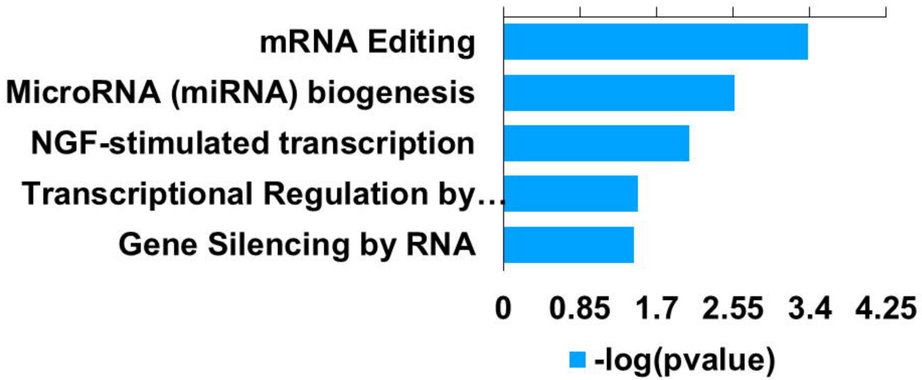

ADAR	*AGO2*	*TRIB1*	*KAT6A*	*AGO2*	*HIPK2*

Only hypomethylated genes

(B)

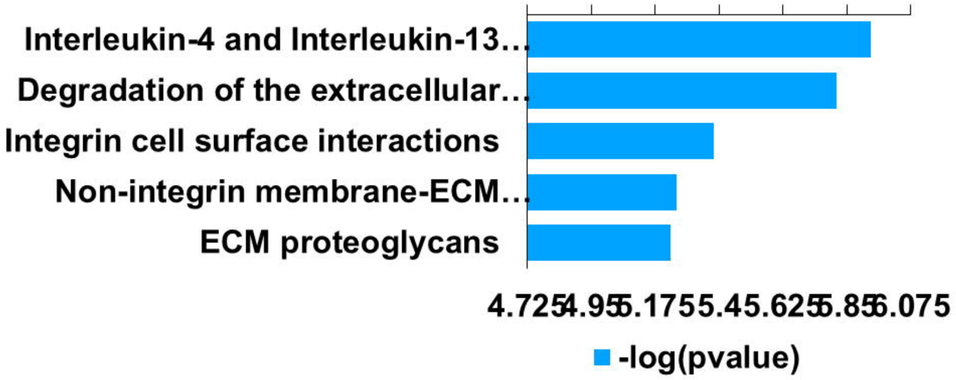

ITGB1	*HSP90AA1*	*MMP2*	*FN1*	*RORA*	*PIK3R1*	*VEGFA*
COL1A2	*ZEB1*	*BCL6*	*S1PR1*	*IL12A*	*CD36*	*VIM*
JUNB	*COL15A1*	*MME*	*HTRA1*	*LAMC2*	*LAMC1*	*NID1*
ADAMTS4	*COL1A1*	*CTSL*	*ADAMTS1*	*COL5A2*	*TIMP2*	*CAPN2*
MMP19	*COL6A3*	*JAM3*	*ITGB5*	*TNC*	*THBS1*	*ITGA8*
PECAM1	*PELO*	*ITGA9*	*APP*	*SPARC*	*LRP10*	

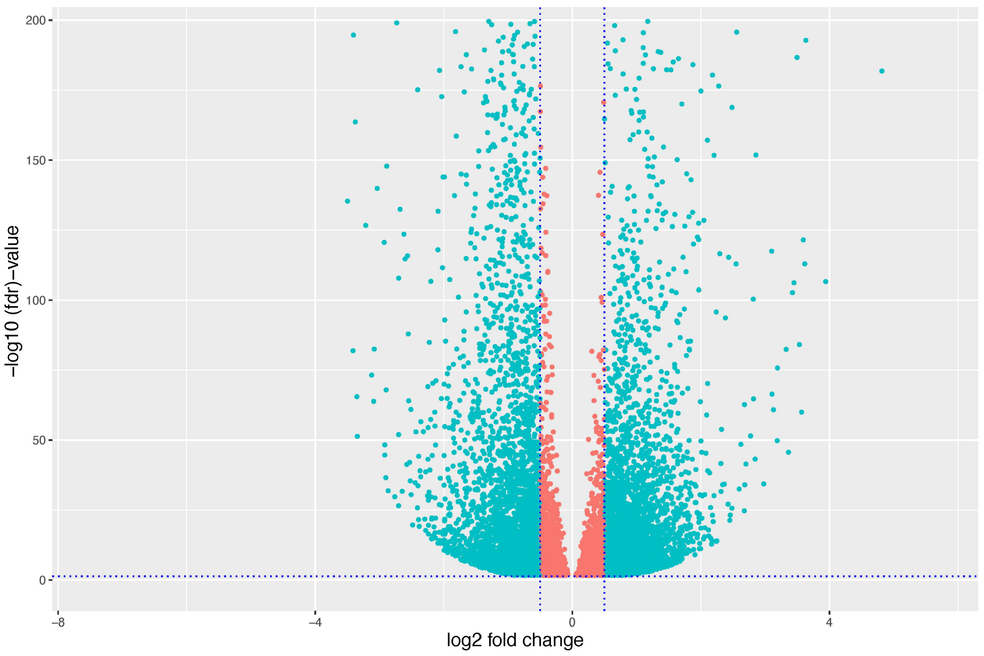

(A)

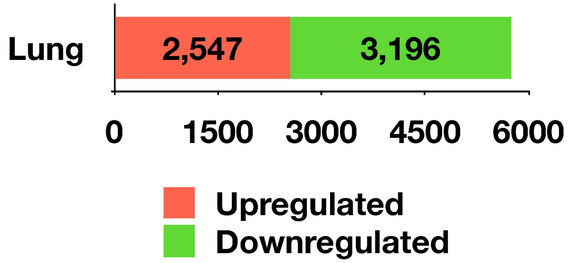

(B)

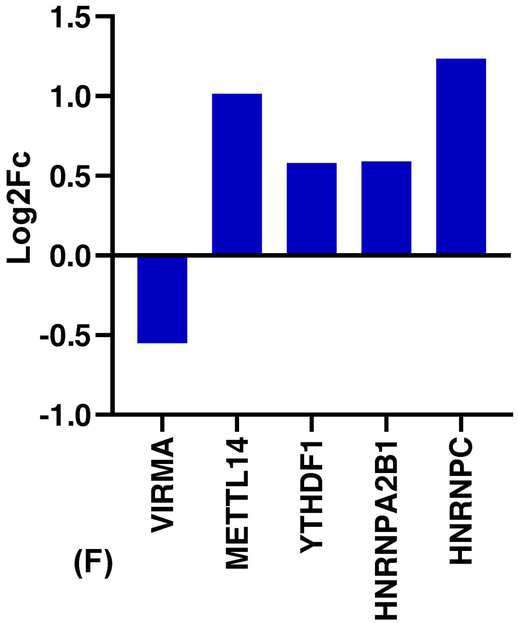

(F)

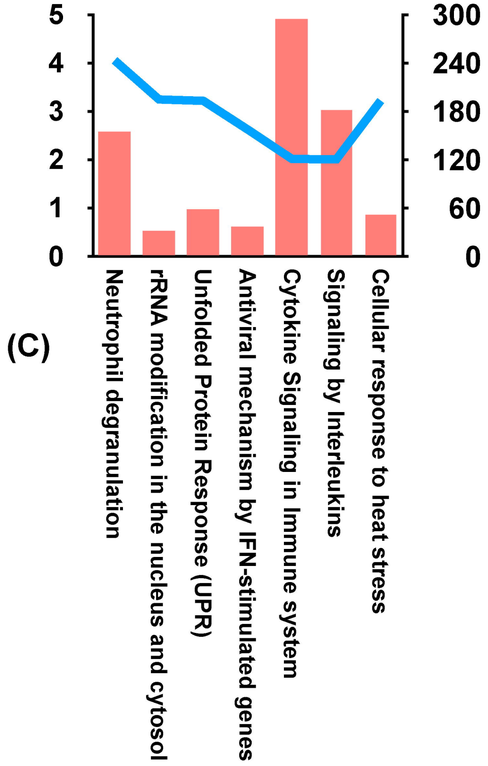

(C)

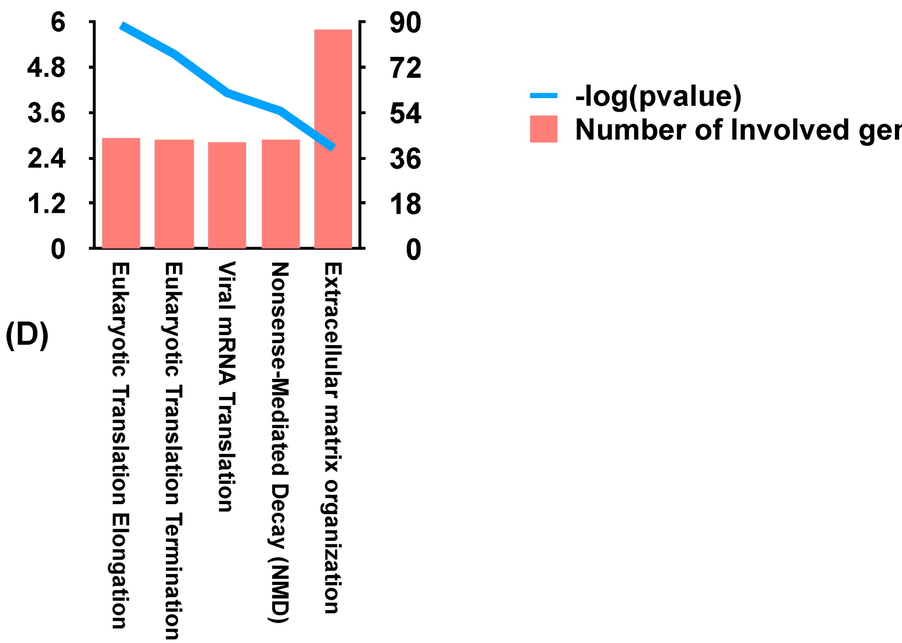

(D)

Stress response genes

GPX2	GPX8	HIF1A	HSP90AA1	HSPA13	HSPH1	SOD2
2.2	1.6	2.0	1.1	1.6	2.5	2.5

Inteferon stimulated genes

IFI44L	IFI6	IFIT1	IFIT2	IFIT3	IFIT5	IRF7	ISG15	ISG20	MX1	OAS1
1.7	1.5	2.0	1.7	1.7	1.3	0.6	0.9	1.2	1.3	0.67

Interleukins

IL17RA	IL18	IL1RN	IL4R	IL7R	IL10RB	IL17RB	IL1R2	IL1RL1	IL27	IL27RA	IL33	IL6ST
0.6	0.6	2.0	0.5	0.6	0.6	2.8	1.1	1.1	1.2	0.7	0.7	0.9

Viral Sensors

DDX58	IFIH1	TLR2	TLR3	TLR4	TLR6
1.5	1.1	1.5	1.3	0.6	1.0

RNA Translation

RPLP1	RPS17	RPL35A	RPS21	RPL11	RPL22
-1.7	-1.2	-1.2	-1.1	-1.1	-1.0

Extracellular matrix

ITGAD	COL8A2	PHYKPL	LOXL1	COL16A1
-3.2	-1.7	-1.5	-1.5	-1.4

(E)

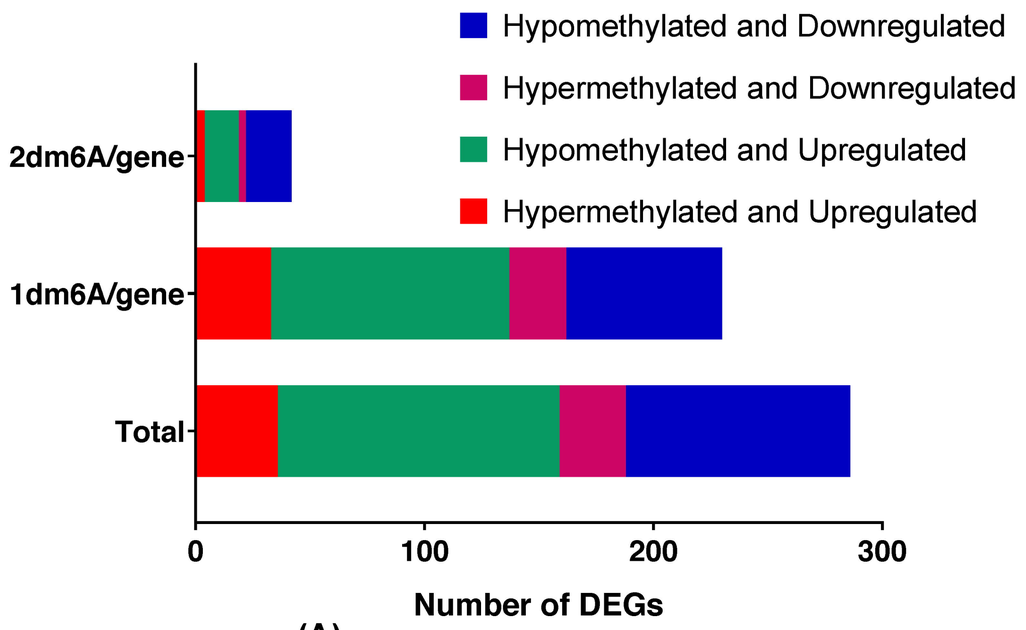

(A)

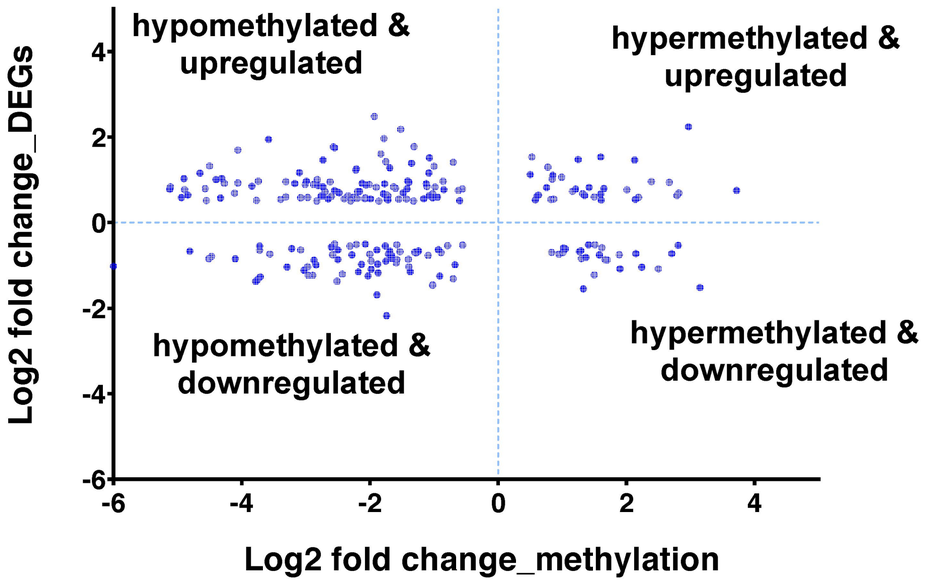

(B)

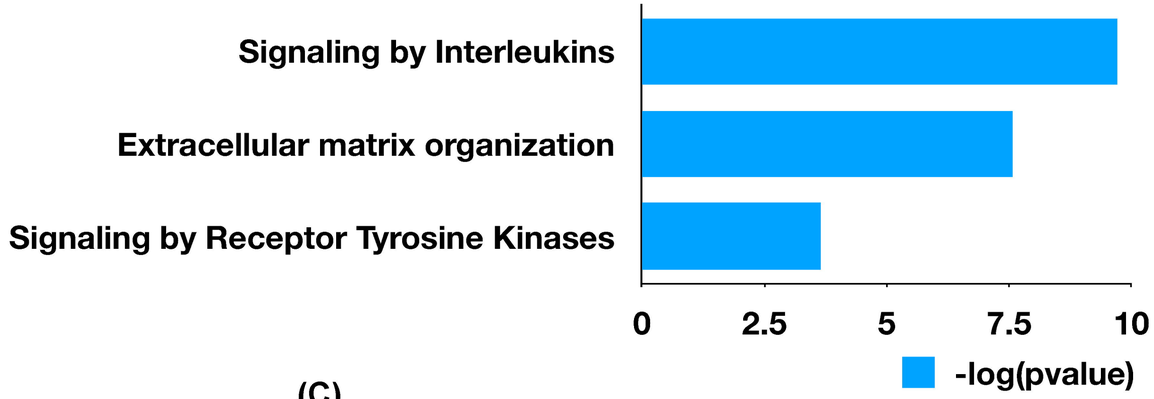

(C)

(D)

Gene	Diff.log2.fc (Methylation)			Diff. Log.fc (Expression)
	Site 1	Site 2	Site 3	
C1QA	-1.3	-1.72	-1.15	-0.54
IL17RA	-2.04	-3.43		0.6
IL1R2	0.99			1.06
IL7R	1.35			0.63
IRF2BP2	-1.02			0.58
OAS1	1.06	1.35		0.67
PDGFRA	-1.72			0.63
TGFBR2	-1.26	-0.82		0.78
HSP90AA1	-1.87	-0.89		1.13
HSPA5	-1.07			1.51
COL15A1	-4.12	-2.18		-0.61
ITGA8	-2.43			-1.21
LOXL1	-2.37	-1.52		-1.51